Synthesis of Spherical Nano- to Microscale Core−Shell Particles $Li[(Ni_{0.8}Co_{0.1}Mn_{0.1})_{1-x}(Ni_{0.5}Mn_{0.5})_x]O_2$ and Their Applications to Lithium Batteries

Yang-Kook Sun,*,† Seung-Taek Myung,‡ Byung-Chun Park,† and Khalil Amine§

Center for Information and Communication Materials, Department of Chemical Engineering, Hanyang University, Seoul 133-791, South Korea, Department of Frontier Materials and Functional Engineering, Graduate School of Engineering, Iwate University, 4-3-5 Ueda, Morioka, Iwate 020-8551, Japan, and Chemical Engineering Division, Argonne National Laboratory, 9700 South Cass Avenue, Argonne, Illinois 60439

Received July 26, 2006
Revised Manuscript Received September 21, 2006

Since the development of the lithium-ion battery by Sony in 1991, $LiCoO_2$ has been most widely used as a positive electrode material because of its easy synthesis and high reversibility in capacity between charge (oxidation) and discharge (reduction). The reversible capacity of $LiCoO_2$ is around 140 mA h g^{-1}.[1] Recent mobile electronic devices need much higher energy density that incorporates multifunctionality. Therefore, the pursuit of high capacity with novel electrode materials for lithium-ion batteries has led to intensive studies of Ni-rich $Li[Ni_{1-x}M_x]O_2$ (M = Co, Al, Mn, etc.).[2−4] By selecting appropriate amounts of Ni and other metal elements, it is possible to deliver high reversible capacity more than 180 or 200 mA h g^{-1}. However, maintenance of the high capacity has seemed to be difficult because of the structural degradation accompanied by oxygen release, and it causes a violent exothermic reaction at a deeply charged state.[5]

In an attempt to stabilize the crystal structure of delithiated $Li_{1-\delta}[Ni_{1-x}Mn_x]O_2$, Spahr et al.[6] introduced a large amount of Mn (50%) for Ni sites in $LiNiO_2$, that is, $Li[Ni_{0.5}Mn_{0.5}]O_2$. Though the large amount of Ni was replaced by Mn, the layered crystal structure was preserved even after high-temperature calcination. The poor electrochemical cycling property was greatly improved by the Mn incorporation. Ohzuku et al.[7] have successfully reproduced and even sophisticatedly improved the material by changing synthetic route. The formal charges for Ni and Mn of the material are 2+ and 4+, respectively.[8] Interestingly, only the $Ni^{2+/3+/4+}$ redox couples for $Li[Ni_{0.5}Mn_{0.5}]O_2$ are electrochemically available;[9] they are accompanied by Li^+ intercalation. On the other hand, the tetravalent Mn remains electrochemically inactive but provides significant structural stability and shows a single-phase transition during repetitive Li^+ deintercalation/intercalation, as confirmed by in situ XRD studies.[10−12] It therefore followed that the onset of the exothermal temperature of deeply delithiated $Li_{1-\delta}[Ni_{1-x}Mn_x]O_2$ was observed usually as high as 280 °C, and heat generation at that temperature was significantly reduced relative to Ni-rich $Li[Ni_{1-x}M_x]O_2$ (M = Mg, Al, Mn, etc.).[13−15] Though it has good structural and thermal properties, the obtained capacity up to 4.3 V versus Li is only 150 mA h g^{-1}, which is quite small compared to Ni-rich $Li[Ni_{1-x}M_x]O_2$ (M = Co, Al, Mn, etc.).[2−4,6]

Though $Li[Ni_{0.5}Mn_{0.5}]O_2$ is fascinating material in terms of structural and thermal stability, the smaller capacity of $Li[Ni_{0.5}Mn_{0.5}]O_2$ relative to Ni-rich $Li[Ni_{0.8}Co_{0.1}Mn_{0.1}]O_2$ should be improved. Surface modifications by heterometal element coatings were not effective enough to increase the reversible capacity, either.[16,17] Among several trials, Li enrichment in the transition metal layer gave the only significant improvement on the electrochemical properties.[12,18] Nonetheless, the obtained capacity was still lower than that of $Li[Ni_{0.8}Co_{0.1}Mn_{0.1}]O_2$. Thus, a combination of both materials, $Li[Ni_{0.5}Mn_{0.5}]O_2$ and $Li[Ni_{0.8}Co_{0.1}Mn_{0.1}]O_2$, would have interesting properties, but a simple blending of the materials would not be preferred in consideration of safety concern, because highly delithiated $Li_{1-\delta}[Ni_{0.8}Co_{0.1}Mn_{0.1}]O_2$ shows a violent exothermic reaction.

The creation of a functional layer on the surface of inorganic particles, the so-called core−shell materials, has attracted a great deal of interest, because core−shell particles show improved physical and chemical properties over their single-component counterparts, and the surface properties of the generated core−shell particles can be altered to meet the required specifications of a broader range of applications.[19] The nanostructured core−shell exhibits several interesting

* Corresponding author. Tel: 82-2-2220-0524. Fax: +82-2-2282-7329. E-mail: yksun@hanyang.ac.kr.
† Hanyang University.
‡ Iwate University.
§ Argonne National Laboratory.

(1) Thomas, M. G. S. R.; David, W. I. F.; Goodenough, J. B.; Groves, P. *Mater. Res. Bull.* **1985**, *20*, 1137.
(2) Broussely, M.; Perton, F.; Biensan, P.; Bodet, J. M.; Lecerf, A.; Delmas, C.; Rougier, A.; Pérès, J. P. *J. Power Sources* **1995**, *54*, 109.
(3) Delmas, C.; Prado, G.; Rougier, A.; Suard, E.; Fournès, L. *Solid State Ionics* **2000**, *135*, 71.
(4) Li, W.; Reimers, J. N.; Dahn, J. R. *Solid State Ionics* **1993**, *67*, 123.
(5) Arai, H.; Okada, S.; Sakurai, Y.; Yamaki, J. *Solid State Ionics* **1998**, *109*, 295.
(6) Spahr, M. E.; Novak, P.; Schnyder, B.; Haas, O.; Nesper, R. *J. Electrochem. Soc.* **1998**, *145*, 1113.
(7) Ohzuku, T.; Makimura, Y. *Chem. Lett.* **2001**, 744.
(8) Ueda, A.; Aoyama, S. In *Proceeding of the 42nd Battery Symposium in Japan*, Yokohama, Japan, 2001; p 130.
(9) Yoon, W.-S.; Grey, C. P.; Balasubramanian, M.; Yang, X.-Q.; McBreen, J. *Chem. Mater.* **2003**, *15*, 3161.
(10) Myung, S.-T.; Komaba, S.; Hosoya, K.; Hirosaki, N.; Miura, Y.; Kumagai, N. *Chem. Mater.* **2005**, *17*, 2427.
(11) Myung, S.-T.; Komaba, S.; Hirosaki, N.; Hosoya, K.; Kumagai, N. *J. Power Sources* **2005**, *146*, 645.
(12) Myung, S.-T.; Komaba, S.; Kurihara, K.; Kumagai, N.; Nakai, I.; Sun, Y.-K.; Yonemura, M.; Kamiyama, T. *Chem. Mater.* **2006**, *18*, 1658.
(13) Reimers, J. N.; Rossen, E.; Jones, C. D.; Dahn, J. R. *Solid State Ionics* **1993**, *61*, 335.
(14) Pouillerie, C.; Croguennec, L.; Biensan, P.; Willmann, P.; Delmas, C. *J. Electrochem. Soc.* **2000**, *147*, 2061.
(15) Jhong, Q.; Sacken, U. V. *J. Power Sources* **1995**, *54*, 221.
(16) Sun, Y.-K.; Hong, K.-J.; Prakash, J. *J. Electrochem. Soc.* **2003**, *150*, A970.
(17) Myung, S.-T.; Izumi, K.; Komaba, S.; Sun, Y.-K.; Yashiro, H.; Kumagai, N. *Chem. Mater.* **2005**, *17*, 3695.
(18) Myung, S.-T.; Komaba, S.; Kumagai, N. *Solid Sate Ionics* **2004**, *170*, 139.
(19) Radtchenko, I. L.; Sukhorukov, G. B.; Gaponik, N.; Kornowski, A.; Rogach, A. L.; Mohwald, H. *Adv. Mater.* **2001**, *13*, 1684.

10.1021/cm061746k CCC: $33.50
Published on Web 10/06/2006

properties in the fields of catalysis, separation technology, microelectronic devices, and biomaterials engineering.[20] So far, a number of methods have been developed for the synthesis of core−shell-structured powders: the layer-by-layer self-assembly process,[21] the hydrothermal precipitation method,[22,23] and the template method.[24]

A possible approach that enables us to maximize the utilization of the high capacity of $Li[Ni_{0.8}Co_{0.1}Mn_{0.1}]O_2$ with improved safety is complete encapsulation of the $Li[Ni_{0.8}Co_{0.1}Mn_{0.1}]O_2$ particle using $Li[Ni_{0.5}Mn_{0.5}]O_2$, which is called core−shell morphology particle, as we reported previously.[25] That is, the high capacity comes from the inner core part of $Li[Ni_{0.8}Co_{0.1}Mn_{0.1}]O_2$, and the outer shell provides significantly enhanced safety. From the above reviews, furthermore, most of core−shell morphologies have just dealt with decades of nanometer scale. It is also expected that variation in the shell thickness may bring about different electrochemical properties. In this paper, therefore, we would like to report on the shell-thickness-controlled core−shell $Li[(Ni_{0.8}Co_{0.1}Mn_{0.1})_{1-x}(Ni_{0.5}Mn_{0.5})_x]O_2$ particles from nanometer to micrometer scale.

Core−shell hydroxides were prepared by a coprecipitation method. Details of the preparation method are described in our previous paper.[25,26] To synthesize the spherical core, we first used appropriate amounts of $NiSO_4 \cdot 6H_2O$, $CoSO_4 \cdot 7H_2O$, and $MnSO_4 \cdot H_2O$ (8:1:1 Ni:Co:Mn cationic ratio) as the starting materials. The starting aqueous solutions were pumped into a continuously stirred tank reactor (CTSR, capacity of 4 L) under a nitrogen atmosphere and reacted with NaOH solution (aq) as the pH control agent and the desired amount of NH_4OH solution (aq) as the chelating agent in the reactor, leading to $[Ni_{0.8}Co_{0.1}Mn_{0.1}](OH)_2$. Ni- and Mn-containing aqueous solution (1:1 Ni:Mn cationic ratio) was continuously pumped into the coprecipitation reactor to encapsulate the $[Ni_{0.8}Co_{0.1}Mn_{0.1}](OH)_2$ core completely. At this stage, to control the shell thickness, the reaction time of the prepared core with Ni and Mn (1:1 Ni:Mn cationic ratio) containing aqueous solutions were controlled from 10 min to 4 h. The precipitated powders were gathered from each reactor as a function of reaction time. The collected powders were carefully washed with deionized water and dried at 25 °C in a vacuum state to remove adhered water completely. Such obtained $[NiCoMn](OH)_2$ compounds were thoroughly mixed with appropriate $LiOH \cdot H_2O$ and heated at 770 °C for 12 h in air. The chemical compositions of the resulting powders were analyzed by atomic absorption spectroscopy (AAS, Vario 6, Analyticjena). X-ray diffractometry (XRD, Rigaku Rint 2200) was employed to characterize the prepared powders. XRD data were obtained at $2\theta = 10-80°$, with a step size of 0.03°

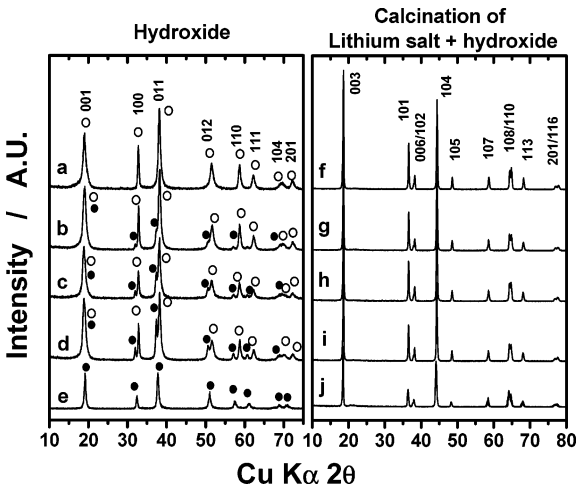

Figure 1. Powder XRD patterns: as-prepared (a) $[Ni_{0.8}Co_{0.1}Mn_{0.1}](OH)_2$; $[Ni_{0.8}Co_{0.1}Mn_{0.1}](OH)_2$ encapsulated by $[Ni_{0.5}Mn_{0.5}](OH)_2$ for (b) 2, (c) 3, and (d) 4 h, and (e) $[Ni_{0.5}Mn_{0.5}](OH)_2$; (f) $Li[Ni_{0.8}Co_{0.1}Mn_{0.1}]O_2$; (g) thermally lithiated product of (b); (h) lithiated product of (c); (i) lithiated product of (d); and lithiated product of (e).

and a count time of 5 s, using Cu Kα radiation. Using the XRD data, we calculated lattice parameters by a least-squares method. The synthesized powder morphologies were observed by a scanning electron microscope (SEM, JSM 6400, JEOL, Japan). BET surface area measurements were done by the nitrogen adsorption−desorption method (Autosorb-1, QUANTACHROME Instruments).

For fabrication of positive electrodes, the prepared powders were mixed with acetylene black and polyvinylidene fluoride (80:10:10 in weight) in *N*-methylpyrrolidinon. The slurry thus obtained was coated onto Al foil and dried at 80 °C for 1 day for roll-pressing. The electrodes were dried again at 120 °C for 4 days in a vacuum state prior to use. A 2032 type of coin cell consisted of the positive electrode, lithium foil as the negative electrode. and 1 M $LiPF_6$ in ethylene carbonate−diethyl carbonate (1:1 in volume) as the electrolyte. The cells were charged and discharged between 3.0 and 4.5 V versus Li by applying a current density of 40 mA g^{-1} (60 mA cm^{-2}) at 25 °C.

For differential scanning calorimetry (DSC) experiments, the cells were finally charged to 4.3 V and opened in the Ar-filled dry box. After opening the cell in the Ar-filled dry box carefully, we removed the extra electrolyte from the surface of the electrode, and the electrode materials were recovered from the current collector. A stainless steel sealed pan with a gold plated copper seal (which can withstand 150 atm of pressure before rupturing and has a capacity of 30 μL) was used to collect 3−5 mg samples. The measurements were carried out in a Pyris 1 differential scanning calorimeter (Perkin-Elmer) using a temperature scan rate of 1 °C min^{-1}. The weight was constant in all cases, indicating that there were no leaks during the experiments.

In order to fabricate the core−shell particles in which $Li[Ni_{0.8}Co_{0.1}Mn_{0.1}]O_2$ is completely capsulated by $Li[Ni_{0.5}Mn_{0.5}]O_2$, it is first indispensable to prepare the $[Ni_{0.8}Co_{0.1}Mn_{0.1}](OH)_2$. As we previously reported, optimized preparation conditions such as reaction temperature, solution pH, the amount of chelating agent, etc., resulted in a well-defined layered hydroxide structure, see Figure 1a. Encapsulation of the prepared $[Ni_{0.8}Co_{0.1}Mn_{0.1}](OH)_2$ by $[Ni_{0.5}Mn_{0.5}](OH)_2$

(20) Caruso, F.; Spasova, M.; Susha, A.; Giersig, M.; Caruso, R. A. *Chem. Mater.* **2001**, *13*, 109.
(21) Guo, C. W.; Cao, Y.; Xie, S. H.; Dai, W. L.; Fan, K. N. *Chem.Commun.* **2003**, 700.
(22) Zhang, Y. X.; Li, G. H.; Zhang, L. D. *Inorg. Chem. Commun.* **2004**, *7*, 344.
(23) Yang, Z. Z.; Niu, Z. W.; Lu, Y. F.; Hu, Z. B.; Han, C. C. *Angew. Chem., Int. Ed.* **2003**, *42*, 1943.
(24) Xu, X.; Asher, S. A. *J. Am. Chem. Soc.* **2004**, *126*, 7940.
(25) Sun, Y.-K.; Myung, S.-T.; Kim, M.-H.; Prakash, J.; Amine, K. *J. Am. Chem. Soc.* **2005**, *127*, 13411.
(26) Lee, M.-H.; Kang, Y.-J.; Myung, S.-T.; Sun, Y.-K. *Electrochim. Acta* **2004**, *50*, 939.

confirms the coexistence of two-layered structures, see Figure 1b. Because of the shorter reaction time (1 h), the reflection of $[Ni_{0.5}Mn_{0.5}](OH)_2$ seems to be weaker. With increasing the reaction time, the distinct diffraction peaks of the $[Ni_{0.5}Mn_{0.5}](OH)_2$ phase is clearly observed in lines c and d of Figure 1. The larger ionic radius of Mn^{2+} (0.83 Å[27]) relative to Ni^{2+} (0.69 Å[27]) and Co^{2+} (0.65 Å[27]) brought about slightly greater lattice parameters, because the diffraction peaks were shifted to a lower angle compared with those in lines a and e of Figure 1. The change in the $[Ni_{0.5}Mn_{0.5}](OH)_2$ diffraction area clearly suggests that the amount of $[Ni_{0.5}Mn_{0.5}](OH)_2$ becomes larger with increasing reaction time.

Cross-sections of the prepared powders were observed by SEM. Figure 2a shows the cross-section images of a $[Ni_{0.8}Co_{0.1}Mn_{0.1}](OH)_2$ particle. From the image, one can imagine that the prepared hydroxide is spherical and consists of only core material. The observed particle size is estimated to be around 10 μm in diameter. Capsulation of $[Ni_{0.8}Co_{0.1}Mn_{0.1}](OH)_2$ by $[Ni_{0.5}Mn_{0.5}](OH)_2$ was done for 20 min, and the result is shown in Figure 2b. From the image we can see that the shell surrounding the core is quite slim (about 200 nm in thickness). Though the core size of the $[Ni_{0.8}Co_{0.1}Mn_{0.1}](OH)_2$ is quite close to from Figure 2a−f, the extended reaction time resulted in more piling of the $[Ni_{0.5}Mn_{0.5}](OH)_2$ on the surface of $[Ni_{0.8}Co_{0.1}Mn_{0.1}](OH)_2$ in Figure 2b−f. The measured shell thickness varied from 200 to 600 nm during reaction for 1 h. The thickness of the shell was around 800 nm for a reaction time of 2 h. The measured shell thicknesses for 3 and 4 h of reaction time are approximately 1 and 1.5 μm, respectively. This means that the change in the shell thickness is facilitated for the 1 h reaction, after which the encapsulation of the core by the shell becomes slower and saturates. It is also very interesting to note that though the reaction was extended to 4 h, the core size remains nearly unchanged. From Figure 2a−f, we can also see that the prepared core−shell hydroxide may not contain pore in both core and shell parts, which indicates that the prepared core−shell particles are quite dense. Chemical compositions were also dependent on the reaction time (Table 1). The longer reaction, in which $[Ni_{0.5}Mn_{0.5}](OH)_2$ is piled more on the $[Ni_{0.8}Co_{0.1}Mn_{0.1}](OH)_2$, brought about an obvious increase in the Mn content. As shown in Figure 1a−e, one can observe the clear separation of the $[Ni_{0.8}Co_{0.1}Mn_{0.1}](OH)_2$ and $[Ni_{0.5}Mn_{0.5}](OH)_2$ phases though the reaction was done longer (Figure 1d). Such a thicker shell led to a stronger reflection in the XRD pattern in lines c and d of Figure 1. From XRD and SEM observations, it was possible to describe the core−shell hydroxide resulting from the core−shell notation (Table 1). In the case of the 4 h reaction, for example, the measured chemical composition was $[Ni_{0.719}Co_{0.073}Mn_{0.208}](OH)_2$ and can be written again as having a core−shell notation of $[(Ni_{0.8}Co_{0.1}Mn_{0.1})_{0.73}(Ni_{0.5}Mn_{0.5})_{0.27}](OH)_2$.

The as-synthesized core−shell hydroxide was fired with a stoichiometric amount of lithium hydroxide at 770 °C for 12 h in air. For comparison, $Li[Ni_{0.8}Co_{0.1}Mn_{0.1}]O_2$ was also synthesized by calcination a mixture of $[Ni_{0.8}Co_{0.1}Mn_{0.1}](OH)_2$ and $LiOH{\cdot}H_2O$ at 770 °C for 12 h in air. The XRD patterns of the produced powders are shown in Figure 1f−j. Calcination of $[Ni_{0.8}Co_{0.1}Mn_{0.1}](OH)_2$ and $LiOH{\cdot}H_2O$ gave rise to the well-ordered rock salt type layered structure (space group $R\bar{3}m$) in Figure 1f. In the case of core−shell hydroxides calcined with lithium salt, one can also observe a similar layered structure as a result of calcination of $[Ni_{0.8}$-

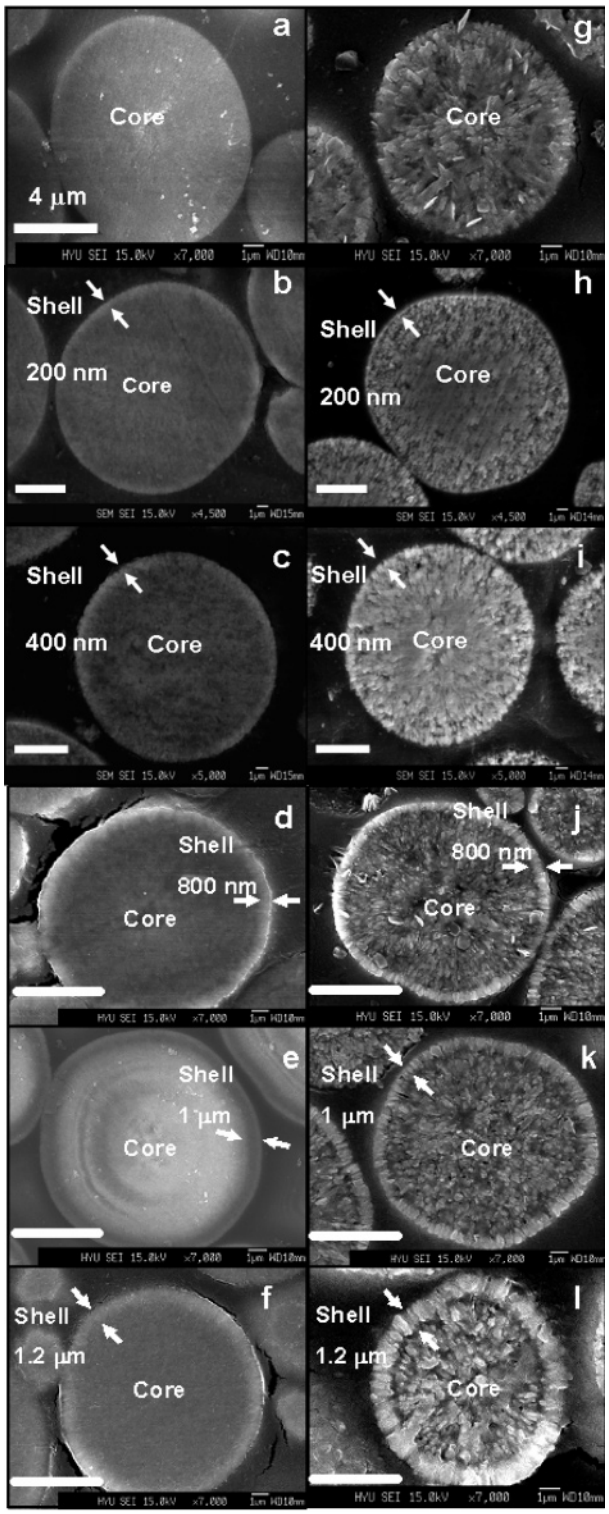

Figure 2. SEM cross-section images: as-prepared (a) $[Ni_{0.8}Co_{0.1}Mn_{0.1}](OH)_2$; $[Ni_{0.8}Co_{0.1}Mn_{0.1}](OH)_2$ encapsulated by $[Ni_{0.5}Mn_{0.5}](OH)_2$ for (a) 20 min, (c) 40 min, (d) 2 h, (e) 3 h, (f) 4 h; (g) core $Li[Ni_{0.8}Co_{0.1}Mn_{0.1}]O_2$; (h) thermally lithiated product of (b); (i) lithiated product of (c); (j) lithiated product of (d); (k) lithiated product of (e); and (k) lithiated product of (f). The scale bar means 4 μm.

(27) Shannon, R. D. *Acta Crystallogr., Sect. A* **1976**, *32*, 751.

Table 1. Comparison of Chemical Compositions of the As-Prepared Hydroxide and Thermally Lithiated Core−Shell Powders.

reaction time (h)	AAS results for as-prepared hydroxide	core−shell notation of the as-prepared hydroxide	chemical compositions for the lithiated core−shell powders after calcination	lattice parameters of lithiated core−shell powders after calcination[a]	
				a axis (Å)	*c* axis (Å)
0	$[Ni_{0.8}Co_{0.1}Mn_{0.1}](OH)_2$	$[Ni_{0.8}Co_{0.1}Mn_{0.1}](OH)_2$	$Li[Ni_{0.8}Co_{0.1}Mn_{0.1}]O_2$	2.8728(5)	14.2336(31)
2	$[Ni_{0.776}Co_{0.092}Mn_{0.132}](OH)_2$	$[(Ni_{0.8}Co_{0.1}Mn_{0.1})_{0.92}(Ni_{0.5}Mn_{0.5})_{0.08}](OH)_2$	$Li[(Ni_{0.8}Co_{0.1}Mn_{0.1})_{0.92}(Ni_{0.5}Mn_{0.5})_{0.08}]O_2$	2.8747(4)	14.2474(24)
3	$[Ni_{0.74}Co_{0.08}Mn_{0.18}](OH)_2$	$[(Ni_{0.8}Co_{0.1}Mn_{0.1})_{0.8}(Ni_{0.5}Mn_{0.5})_{0.2}](OH)_2$	$Li[(Ni_{0.8}Co_{0.1}Mn_{0.1})_{0.8}(Ni_{0.5}Mn_{0.5})_{0.2}]O_2$	2.8778(6)	14.2538(33)
4	$[Ni_{0.719}Co_{0.073}Mn_{0.208}](OH)_2$	$[(Ni_{0.8}Co_{0.1}Mn_{0.1})_{0.73}(Ni_{0.5}Mn_{0.5})_{0.27}](OH)_2$	$Li[(Ni_{0.8}Co_{0.1}Mn_{0.1})_{0.73}(Ni_{0.5}Mn_{0.5})_{0.27}]O_2$	2.8788(5)	14.2545(28)
0	$[Ni_{0.5}Mn_{0.5}](OH)_2$	$[Ni_{0.5}Mn_{0.5}](OH)_2$	$Li[Ni_{0.5}Mn_{0.5}]O_2$	2.8814(6)	14.2719(10)

[a] The calculation of the lattice parameters were carried out by a least-square method.

$Co_{0.1}Mn_{0.1}](OH)_2$ and $LiOH{\cdot}H_2O$ in Figure 1g−i. Because of the structural similarity between $Li[Ni_{0.8}Co_{0.1}Mn_{0.1}]O_2$ and $Li[Ni_{0.5}Mn_{0.5}]O_2$, calcinations resulting from $[Ni_{0.8}Co_{0.1}Mn_{0.1}](OH)_2$ and $LiOH{\cdot}H_2O$ exhibited overlapping diffraction patterns in Figure 1g−i. From this tendency, we doubted that the core−shell morphology shown in Figure 2b−f might disappear and the shell would be merged into the core or vice versa. Thus, the cross-sections of the thermally lithiated resultant powders were observed by SEM and the results are shown in Figure 2h−l. The cross-section image of $Li[Ni_{0.8}Co_{0.1}Mn_{0.1}]O_2$ showed that the spherical secondary morphology was maintained, as expected, and the secondary particle is composed by submicrometer primary particles in Figure 2g, resulting from the high-temperature calcination of the core−shell hydroxide. Surprisingly, the core−shell morphology was preserved even after firing at higher temperature in Figure 2h−l. Furthermore, the thickness of the shells remained nearly unchanged compared to those of the core−shell hydroxides in Figure 2b−f, though the core−shell powders were heat-treated at higher temperature. This indicates that the lithium element was readily incorporated into the dehydrated oxide matrix and finally brought about the lithiated $Li[(Ni_{0.8}Co_{0.1}Mn_{0.1})_{1-x}(Ni_{0.5}Mn_{0.5})_x]O_2$. The measured BETs for the synthesized powders ranged from 0.55 to 0.65 $m^2\ g^{-1}$, with varying shell thickness. Chemical compositions of the thermally lithiated powders also exhibited the same compositions as those of the core−shell hydroxides for the transition metal components (Table 1). From these results, it is evident that the core−shell $Li[(Ni_{0.8}Co_{0.1}Mn_{0.1})_{1-x}(Ni_{0.5}Mn_{0.5})_x]O_2$ particle consists of $Li[Ni_{0.8}Co_{0.1}Mn_{0.1}]O_2$ as the core and $Li[Ni_{0.5}Mn_{0.5}]O_2$ as the shell. Similar to the hydroxides, the variation in the lattice parameters also increased in both the *a* and *c* axes with increasing amounts of $Li[Ni_{0.5}Mn_{0.5}]O_2$ (Table 1), because of the difference in the ionic radius of transition metal elements. By employing the spherical hydroxide, it was also possible to control the shell thickness from a nano- to microscale core−shell particle.

To know the functionality of the lithiated core−shell powders, $Li[(Ni_{0.8}Co_{0.1}Mn_{0.1})_{1-x}(Ni_{0.5}Mn_{0.5})_x]O_2$, we examined electrochemical properties. Figure 3 illustrates the initial charge and discharge curves of $Li[(Ni_{0.8}Co_{0.1}Mn_{0.1})_{1-x}(Ni_{0.5}Mn_{0.5})_x]O_2$ ($x = 0-0.27$). The applied current density across the positive electrodes was 40 mA g^{-1} (60 mA cm^{-2}) at 25 °C. $Li[(Ni_{0.8}Co_{0.1}Mn_{0.1}]O_2$ showed three or four distinct voltage plateaus. The achieved capacity on discharge was approximately 212 mA h g^{-1}, and the initial coulombic efficiency between charge and discharge capacity for the core $Li[Ni_{0.8}Co_{0.1}Mn_{0.1}]O_2$ was around 85%, which is an ordinary value for the current compound.[5] As the core, $Li[(Ni_{0.8}Co_{0.1}$-

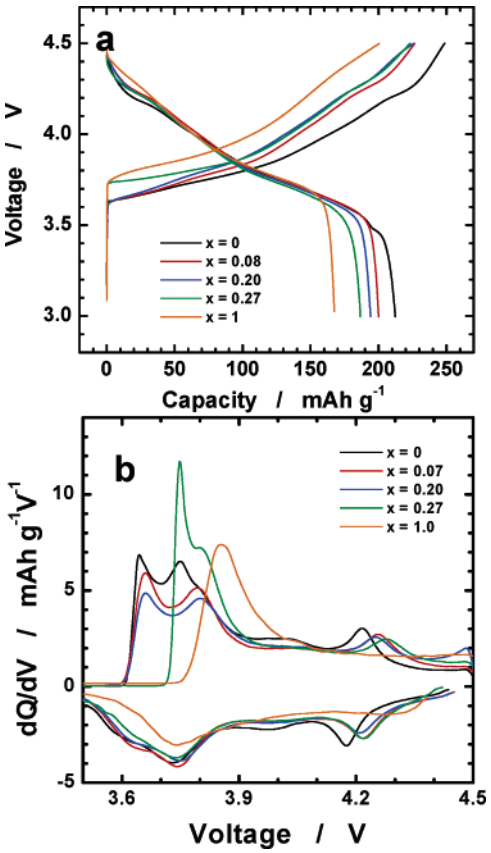

Figure 3. (a) Initial charge and discharge curves of $Li/Li[(Ni_{0.8}Co_{0.1}Mn_{0.1})_{1-x}(Ni_{0.5}Mn_{0.5})_x]O_2$ ($x = 0-0.27$) and (b) their differentiated curves for the composition.

$Mn_{0.1}]O_2$, was encapsulated by the $Li[Ni_{0.5}Mn_{0.5}]O_2$ shell ($x = 0.08$ in $Li[(Ni_{0.8}Co_{0.1}Mn_{0.1})_{1-x}(Ni_{0.5}Mn_{0.5})_x]O_2$), the obtained initial charge and discharge capacity decreased compared to that of $Li[(Ni_{0.8}Co_{0.1}Mn_{0.1}]O_2$. However, the initial efficiency was slightly improved to 88.1 from 85%. As the shell became thicker, the delivered charge capacities were similar, but the thicker shell had a slightly lower discharge capacity (Figure 3a). Furthermore, the initial efficiency was lowered with increasing shell thickness. The trend would come from the intrinsic electrochemical property of $Li[Ni_{0.5}Mn_{0.5}]O_2$, which usually shows a relatively large irreversibility between the first charge and discharge of about 75% when it cycles to 4.6 V versus Li.[10−12] In our case, the $Li/Li[Ni_{0.5}Mn_{0.5}]O_2$ cell had 83% initial reversibility (Figure 3a). One striking feature is the operation voltage above 3.7 V on charge for $x = 0.08$ and 0.20 in $Li[(Ni_{0.8}Co_{0.1}Mn_{0.1})_{1-x}(Ni_{0.5}Mn_{0.5})_x]O_2$, though the operation voltages on discharge were similar regardless of composition in Figure 3a. The characteristic can be observed clearly in the *dQ*/*dV* derivative

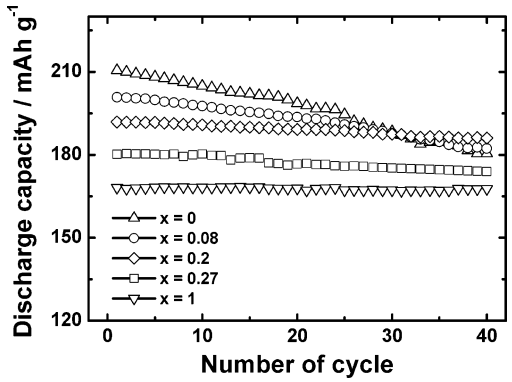

Figure 4. Cyclability of Li/Li[$(Ni_{0.8}Co_{0.1}Mn_{0.1})_{1-x}(Ni_{0.5}Mn_{0.5})_x$]$O_2$ (x = 0−1).

curves in Figure 3b. For comparison, the dQ/dV derivative curve of Li[$Ni_{0.5}Mn_{0.5}$]O_2 was added in Figure 3b. The capacity at around 3.65 V was smaller for the core−shell particles on charge (Figure 3b), which means that the portion of Li[$Ni_{0.8}Co_{0.1}Mn_{0.1}$]O_2 is reduced in the core−shell Li[$(Ni_{0.8}Co_{0.1}Mn_{0.1})_{1-x}(Ni_{0.5}Mn_{0.5})_x$]$O_2$ particle. Li[$Ni_{0.8}Co_{0.1}$-$Mn_{0.1}$]O_2 also had a more or less higher capacity at 3.75 V. However, the core−shell particle shows the capacity at slightly higher voltages, 3.8 and 4.25 V on charge. On discharge, the reversible behaviors are also observed. When the derivative curve is compared with that of Li[$Ni_{0.5}Mn_{0.5}$]-O_2, the reason is reasonable, because Li[$Ni_{0.5}Mn_{0.5}$]O_2 exhibits a relatively higher capacity at ca. 3.8 V on charge (Figure 3b). For x = 0.27 in Li[$(Ni_{0.8}Co_{0.1}Mn_{0.1})_{1-x}(Ni_{0.5}$-$Mn_{0.5})_x$]$O_2$, especially, charge begins at a relatively higher voltage of around 3.7 V, which is quite similar behavior to Li[$Ni_{0.5}Mn_{0.5}$]O_2, though the material has a higher capacity than that of Li[$Ni_{0.5}Mn_{0.5}$]O_2 because the Li[$Ni_{0.8}Co_{0.1}Mn_{0.1}$]-O_2 delivers a higher capacity. As shown in Figure 2h, the material has a thicker shell by approximately 1.5 μm. From these results, it is inferred that the core−shell particle would prefer to behave depending on the shell thickness. That is, a thin-shelled particle has similar properties to the core material and a thick-shelled particle prefers to have the shell material character.

Figure 4 shows electrochemical cycling results plotted by discharge capacity versus cycle number up to 4.5 V. As is well-known,[28] the core Li[$Ni_{0.8}Co_{0.1}Mn_{0.1}$]O_2 material exhibited severe capacity fading, ~0.75 mA h (g of oxide)$^{-1}$ per cycle (85% retention) in Figure 4. Nanoscale core−shell particles (<500 nm shell thickness) showed a trend similar to that of the core material. A small amount of Li[$Ni_{0.5}Mn_{0.5}$]-O_2 (x = 0.08) capsulation for Li[$Ni_{0.8}Co_{0.1}Mn_{0.1}$]O_2 resulted in quite improved cyclability (91% retention at the 40th cycle). For x = 0.2 in Li[$(Ni_{0.8}Co_{0.1}Mn_{0.1})_{1-x}(Ni_{0.5}Mn_{0.5})_x$]$O_2$, the capacity retention was greatly improved to 98 from 85% at the 40th cycle, compared with the core Li[$Ni_{0.8}Co_{0.1}Mn_{0.1}$]-O_2. Similar tendencies were also observed in much thicker core−shell powders, Li[$(Ni_{0.8}Co_{0.1}Mn_{0.1})_{0.73}(Ni_{0.5}Mn_{0.5})_{0.27}$]-$O_2$, and the shell material as well, showing 98% capacity retention of their initial capacities (Figure 4). As expected, the smaller capacity of the shell material reflects the reduction

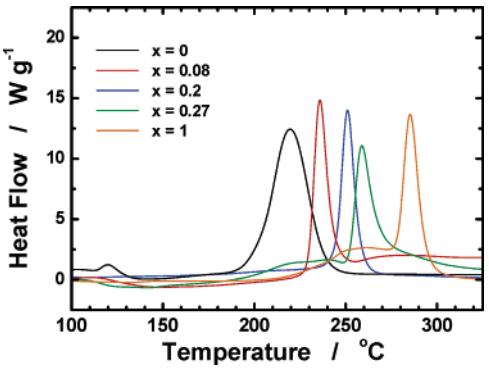

Figure 5. DSC profiles of the Li[$(Ni_{0.8}Co_{0.1}Mn_{0.1})_{1-x}(Ni_{0.5}Mn_{0.5})_x$]$O_2$ (x = 0−1) electrodes charged to 4.5 V versus Li

of obtainable capacity in the core−shell material. On the other hand, surprisingly, it provides a significant structural stability at a highly delithiated state[10−12] so that the thick-shelled Li[$(Ni_{0.8}Co_{0.1}Mn_{0.1})_{1-x}(Ni_{0.5}Mn_{0.5})_x$]$O_2$ ($x \geq 0.2$) enables us to retain the higher discharge capacity upon electrochemical cycling.

Figure 5 exhibits DSC profiles of theLi[$(Ni_{0.8}Co_{0.1}Mn_{0.1})_{1-x}$-$(Ni_{0.5}Mn_{0.5})_x$]$O_2$ (x = 0−1) electrodes charged to 4.5 V versus Li. As pointed out by Arai et al.,[5] the Ni-rich Li[$Ni_{0.8}Co_{0.1}$-$Mn_{0.1}$]O_2 core material had a lower exothermic onset temperature around 190 °C, and the main exothermic reaction occurred at about 220 °C, showing quite a broad reaction range in Figure 5. Such reaction is generally accompanied by the oxygen release from the host oxide matrix. Interestingly, the simple encapsulation of the core by Li[$Ni_{0.5}Mn_{0.5}$]-O_2 led to the significant improvement of the onset exothermic temperature to 230 from 190 °C for Li[$(Ni_{0.8}Co_{0.1}Mn_{0.1})_{1-x}$-$(Ni_{0.5}Mn_{0.5})_x$]$O_2$ (x = 0.08). The reaction range appeared to be quite narrow and sharp. The onset and main exothermic temperatures increased monotonously, and the accompanying heat generation was fairly reduced by increasing the shell thickness of the core−shell powders in Figure 5. It is reasonable because the highly oxidized $Li_{1-\delta}$[$Ni_{0.5}Mn_{0.5}$]O_2 delayed the reaction temperature to approximately 290 °C with reduced heat generation. Here, we can think that if the core−shell powders are not formed but Li[$Ni_{0.8}Co_{0.1}Mn_{0.1}$]-O_2 is mixed, we may observe the separated exothermic reactions corresponding to each material. However, one can clearly see the simultaneous increase in the exothermic temperature and lowering of the heat generation from the thickness-controlled core−shell Li[$(Ni_{0.8}Co_{0.1}Mn_{0.1})_{1-x}$ $(Ni_{0.5}Mn_{0.5})_x$]O_2 (x = 0−1) (Figure 5). Such behaviors were possible because of the existence of the complete capsulation of Li[$Ni_{0.8}Co_{0.1}Mn_{0.1}$]O_2 by the thermally stable Li[$Ni_{0.5}Mn_{0.5}$]-O_2 powders.

Detailed studies are underway to elucidate the charge and discharge mechanism of the core−shell Li[$(Ni_{0.8}Co_{0.1}Mn_{0.1})_{1-x}$ $(Ni_{0.5}Mn_{0.5})_x$]O_2. The synergetic effects of spherical core−shell particles as lithium storage materials open a new era for the development of lithium batteries with a high capacity, excellent cyclability, and high thermal stability.

Acknowledgment. This work was supported by the University IT Research Center Project.

CM061746K

(28) Cho, J.; Kim, T.-J.; Kim, J.; Noh, M.; Park, B. *J. Electrochem. Soc.* **2004**, *151*, A1899.